Inorganic Chemistry
Article

Inorg. Chem. **2011**, *50*, 1213–1219 **1213**
DOI: 10.1021/ic1015252

A Highly Selective Fluorescent Chemosensor for Zinc Ion and Imaging Application in Living Cells

Uday Chand Saha,[⊥] Basab Chattopadhyay,[†] Koushik Dhara,*[,‡] Sushil Kumar Mandal,[§] Sandipan Sarkar,[⊥] Anisur Rahman Khuda-Bukhsh,[§] Monika Mukherjee,[†] Madeleine Helliwell,[¶] and Pabitra Chattopadhyay*[,⊥]

[⊥]Department of Chemistry, Burdwan University, Golapbug, Burdwan 713104, West Bengal, India, [†]Department of Solid State Physics, Indian Association for the Cultivation of Science, Jadavpur, Kolkata 700032, India, [‡]Department of Chemistry, Sambhu Nath College, Labpur, Birbhum 731303, West Bengal, India, [§]Cytogenetics and Molecular Biology Laboratory, Department of Zoology, University of Kalyani, Kalyani 741235, India, and [¶]Department of Chemistry, University of Manchester, Manchester M13 9PL, United Kingdom

Received July 29, 2010

A new 2,6-bis(5,6-dihydrobenzo[4,5]imidazo[1,2-*c*]quinazolin-6-yl)-4-methylphenol (**1**) serves as a highly selective and sensitive fluorescent probe for Zn^{2+} in a HEPES buffer (50 mM, DMSO:water = 1:9 (v/v), pH = 7.2) at 25 °C. The increase in fluorescence in the presence of Zn^{2+} is accounted for by the formation of dinuclear Zn^{2+} complex $[Zn_2(C_{35}H_{25}N_6O)(OH)(NO_3)_2(H_2O)]$ (**2**), characterized by X-ray crystallography. The fluorescence quantum yield of the chemosensor **1** is only 0.019, and it increases more than 12-fold (0.237) in the presence of 2 equiv of the zinc ion. Interestingly, the introduction of other metal ions causes the fluorescence intensity to be either unchanged or weakened. By incubation of cultured living cells (A375 and HT-29) with the chemosensor **1**, intracellular Zn^{2+} concentrations could be monitored through selective fluorescence chemosensing.

Introduction

Zinc, being the second-most abundant transition metal in the human body for sustaining life, plays a pivotal role in controlling gene transcription and metalloenzyme function.[1,2] The cellular zinc ion concentration varies from the nanomolar range to about 0.3 mM.[3] Several organs, e.g., brain,[4] pancreas,[5] spermatozoa,[6] vesicles of presynaptic neurons,[7] etc., contain zinc in either a free state or a sequestered form. Disruption of Zn^{2+} homeostasis may play a role in the pathology of several neurodegenerative disorders,[8a,b] like the formation of amyloid plaques in Alzheimer's disease.[8c−e] Synaptic vesicles in excitatory nerve terminals contain high concentrations of chelatable Zn^{2+}, which is released by neuronal activity.[9] Although it is recognized that Zn^{2+} has many important cellular functions, its physiological significance is not completely understood.

The fluorescent detection and imaging of target biological molecules of interest in living systems have become an active topic in many fields via fluorescence microscopy.[10] Many fluorescent dyes have been engineered as useful sensors for imaging biologically active Zn^{2+}. To date, the common probes are derivatives of 8-aminoquinoline,[11] Zinquin,[12]

*To whom correspondence should be addressed. E-mail: koushikdhara@rediffmail.com (K.D.), pabitracc@yahoo.com (P.C.).

(1) Vallee, B. L.; Falchuk, K. H. *Physiol. Rev.* **1993**, *73*, 79.
(2) Auld, D. S. *BioMetals* **2001**, *14*, 271.
(3) Lippard, S. J.; Berg, J. M. *Principles of Bioinorganic Chemistry*; University Science Books: Mill Valley, CA, 1994.
(4) (a) Li, Y.; Hough, C.; Sarvey, J. *Sci. STKE* **2003**, *182*, 19. (b) Frederickson, C. J.; Bush, A. I. *BioMetals* **2001**, *14*, 353. (c) Frederickson, C. J. *Int. Rev. Neurobiol.* **1989**, *31*, 145.
(5) (a) Qian, W. J.; Gee, K. R.; Kennedy, R. T. *Anal. Chem.* **2003**, *75*, 3468. (b) Zalewski, P. D.; Millard, S. H.; Forbes, I. J.; Kapaniris, O.; Slavotinek, A.; Betts, W. H.; Ward, A. D.; Lincoln, S. F.; Mahadevan, I. *J. Histochem. Cytochem.* **1994**, *42*, 877.
(6) Zalewski, P. D.; Jian, X.; Soon, L. L. L.; Breed, W. G.; Seamark, R. F.; Lincoln, S. F.; Ward, A. D.; Sun, F. Z. *Reprod., Fertil. Dev.* **1996**, *8*, 1097.
(7) (a) Assaf, S. Y.; Chung, S. H. *Nature* **1984**, *308*, 734. (b) Howell, G. A.; Welch, M. G.; Frederickson, C. J. *Nature* **1984**, *308*, 736.
(8) (a) Cuajungco, M. P.; Lees, G. J. *Neurobiol. Dis.* **1997**, *4*, 137. (b) Bush, A. I. *Curr. Opin. Chem. Biol.* **2000**, *4*, 184. (c) Suh, S. W.; Jensen, K. B.; Jensen, M. S.; Silva, D. S.; Kesslak, P. J.; Danscher, G.; Frederiskson, C. J. *Brain Res.* **2000**, *852*, 274. (d) Curtain, C. C.; Ali, F.; Volitakis, I.; Cherny, R. A.; Norton, R. S.; Beyreuther, K.; Barrow, C. J.; Masters, C. L.; Bush, A. I.; Barnham, K. J. *J. Biol. Chem.* **2001**, *276*, 20466. (e) Suzuki, K.; Miura, T.; Takeuchi, H. *Biochem. Biophys. Res. Commun.* **2001**, *285*, 991.
(9) Fried, M.; Crothers, D. M. *Nucleic Acids Res.* **1981**, *9*, 6505.
(10) (a) Prasad, P. N. *Introduction to Biophotonics*; Wiley: New York, 2003. (b) Pawley, J. B. *Handbook of Biological Confocal Microscopy*; Plenum: New York, 1995. (c) Lichtman, J. W.; Conchello, J.-A. *Nat. Methods* **2005**, *2*, 910. (d) Xu, Z.; Baek, K.-H.; Kim, H. N.; Cui, J.; Qian, X.; Spring, D. R.; Shin, I.; Yoon, J. *J. Am. Chem. Soc.* **2010**, *132*, 601. (e) Zhou, X.; Yu, B.; Guo, Y.; Tang, X.; Zhang, H.; Liu, W. *Inorg. Chem.* **2010**, *49*, 4002. (f) Xue, Li.; Liu, Q.; Jiang, H. *Org. Lett.* **2009**, *11*, 3454. (g) Liu, Z.; Zhang, C.; Li, Y.; Wu, Z.; Qian, F.; Yang, X.; He, W.; Gao, X.; Guo, Z. *Org. Lett.* **2009**, *11*, 795. (h) Qian, F.; Zhang, C.; Zhang, Y.; He, W.; Gao, X.; Hu, P.; Guo, Z. *J. Am. Chem. Soc.* **2009**, *131*, 1460.
(11) Zhang, Y.; Guo, X.; Si, W.; Jia, L.; Qian, X. *Org. Lett.* **2008**, *10*, 473.

Published on Web 01/19/2011

Zinbo-5,[13] the Zinpyr family,[14] coumarin,[15] and the TQEN family.[16] However, the search for readily accessible fluorescent Zn^{2+} probes with high sensitivity and selectivity is still a challenging task. Thus, the development of fluorescent chemosensors for probing Zn^{2+} has been an active topic as a result of operational simplicity and high sensitivity. To the best of our knowledge, the 5,6-dihydrobenzo[4,5]imidazo[1,2-*c*]-quinazoline (DBIQ)-based fluorescent probe for sensing Zn^{2+} for cellular imaging in living cells is still unexplored, despite the fact that it exhibits a broad spectrum of biological activities.[17]

In this work, we report newly designed 2,6-bis(5,6-dihydrobenzo[4,5]imidazo[1,2-*c*]quinazolin-6-yl)-4-methylphenol (**1**) as a DBIQ-based highly selective and sensitive fluorescent probe for sensing Zn^{2+} in a *N*-2-hydroxyethylpiperazine-*N*′-2-ethanesulfonic acid (HEPES) buffer [50 mM, dimethyl sulfoxide:water = 1:9 (v/v), pH = 7.2] at 25 °C.

Experimental Section

Materials and Physical Methods. All reagents and chemicals were purchased from Sigma and used without further purification. Solvents used for spectroscopic studies were purified and dried by standard procedures before use. Fourier transform infrared (FT-IR) spectra were obtained on a Nicolet Magna-IR 750 spectrometer with samples prepared as KBr pellets. Elemental analysis was carried out in a Perkin-Elmer 2400 Series-II CHN analyzer. Fluorescence and absorption spectra were performed using Hitachi F-4500 fluorescence and Jasco UV/vis/NIR V-570 spectrophotometers, respectively. Fluorescence lifetimes were determined from time-resolved intensity decay by the method of time-correlated single-photon counting using IBM Decay Analysis Software for Windows v6.1.98 and a nano LED at 372 nm as the light source. Electrospray ionization (ESI) mass spectra were recorded on a Qtof Micro YA263 mass spectrometer.

Reagents for Cell Study. Dulbecco's modified Eagle medium (DMEM), fetal bovine serum (FBS), penicillin, streptomycin, neomycin (PSN) antibiotic, trypsin, and ethylenediaminetetraacetic acid (EDTA) were obtained from Gibco BRL (Grand Island, NY). Tissue culture plasticwares were obtained from BD Biosciences (Rockville, MD). All other chemicals used were from Sigma Chemical Co. (St. Louis, MO).

Synthesis of the Chemosensor 1. 2,6-Diformyl-4-methylphenol was synthesized starting from *p*-cresol and following a published procedure.[18] To a solution of 2,6-diformyl-4-methylphenol (0.328 g, 2 mmol) in 30 mL of methanol was added 2-(2-aminophenyl)-1*H*-benzimidazole (0.836 g, 4 mmol) in 20 mL of methanol. The reaction mixture was refluxed for 2 h. The solution was filtered, and a light-yellow product was found after evaporation of the filtrate. It was then dissolved in a *N*,*N*-dimethylformamide (DMF)/water solvent, and after few days, light-yellow X-ray-quality crystals of **1** were obtained in good yield (1.11 g, 87%). Anal. Calcd for $C_{38}H_{35}N_7O_3$: C, 71.57; H, 5.53; N, 15.37. Found: C, 71.23; H, 5.35; N, 15.65. FT-IR (KBr phase, ν_{max}/cm^{-1}): 1678s, 1618s, 1587s. ^1H NMR ($CDCl_3$, 300 MHz, δ ppm): 1.97 (s, 3H), 2.59 (s, 6H), 5.22−5.36 (b, 2H), 6.53 (s, 2H), 6.73−7.79 (m, 18H), 8.17 (s, 1H), 9.85 (s, 1H). ^{13}C NMR ($CDCl_3$, 300 MHz, δ ppm): 20.69, 40.96, 11.88, 114.36, 119.44, 122.46, 123.04, 125.75, 129.91, 130.53, 131.83, 133.07, 141.99, 143.91, 147.54, 151.36, 152.43, 197.59 (see Figure S1 in the Supporting Information). The ESI mass spectrum of **1** (Figure S2 in the Supporting Information) in water shows a peak at *m*/*z* 547.224, which can be assigned to $[M + H]^+$, where M = $C_{35}H_{26}N_6O$.

Synthesis of $[Zn_2(C_{35}H_{25}N_6O)(OH)(NO_3)_2(H_2O)]$ (2). A total of 40 mL of an aqueous solution of $Zn(NO_3)_2 \cdot 6H_2O$ (0.238 g, 0.80 mmol) was added slowly to a stirred solution of 5 mL of dimethyl sulfoxide (DMSO) and the chemosensor **1** (0.255 g, 0.40 mmol) while maintaining the pH at ∼7.2. The mixture was stirred for 30 min, whereby a yellow solution was formed. X-ray-quality single crystals were obtained upon slow evaporation of the solution at ambient temperature after a few days (yield 0.27 g, 82%). Anal. Calcd for $C_{35}H_{28}N_8O_9Zn_2$: C, 50.32; H, 3.38; N, 13.41. Found: C, 50.13; H, 3.27; N, 13.57. FT-IR (KBr phase, ν_{max}/cm^{-1}): 1632s, 1608s, 1597s, 1545s.

X-ray Data Collection and Structure Determination of 1 and 2. X-ray diffraction data for compound **1** were collected at 100(2) K on a Bruker SMART APEX CCD X-ray diffractometer using graphite-monochromated Mo Kα radiation (λ = 0.710 73 Å). The integrated intensities and cell refinement were determined with the *SAINT* software package[19] using a narrow-frame integration algorithm. Structure determination using standard laboratory instruments has not been possible for **2** because of its small crystal size, needle habit, and weak diffraction. The crystal structure of **2** has, therefore, been determined using microcrystalline fragments. Data collection for **2** was performed with silicon 111 monochromated synchrotron radiation (λ = 0.6889 Å) at Beamline I19 of a Diamond Light Source, equipped with a Crystal Logic four-circle κ goniometer and a Rigaku Saturn 724+ CCD detector at T = 150(2) K, using the ω-rotation scan technique with wide frames. There was no deterioration of the crystal during data collection. Data reduction was accomplished using the *d*TREK* software package.[20] Absorption corrections based on multiscans using REQAB within the *d*TREK* software package were applied. Both structures were solved by direct methods with the *SHELXS-97* program.[21] Refinements were carried out by least-squares procedures on F^2, using all data, by application of the *SHELXL-97* program.[21] In compound **1**, one of the DBIQ fragments is disordered into two conformations (*Z* and *E*) by rotation about the C(*p*-cresol)−C(quinazoline) bond with occupancy factors 0.654(4) and 0.346(4), respectively. During anisotropic refinement in *SHELXL*, rigid bond (DELU) restraints on the U_{ij} values were applied. In compound **2**, half of the molecules having bonded nitrate were solvated with a partially occupied water molecule, while the other half had a coordinated water molecule with a free nitrate ion in the lattice. Anisotropic refinement in **2** was restrained using the DELU, SIMU, ISOR, and DFIX options in *SHELXL*. To get an acceptable geometry of the disordered nitrate ions, SADI and FLAT restraints were also applied. In **1**, the H atoms of the solvent water molecule and the H(N1) and H(N4) atoms were located from the difference Fourier map and refined isotropically. All other H atoms in compound **1** as well as in **2** were placed in idealized positions and refined using a riding model. In **2**, the H atoms of the coordinated or solvent water molecules could not be located but are included in the formula.

Fluorimetric Analysis. Fluorescence spectroscopic studies were performed with a Hitachi F-4500 fluorescence spectrophotometer. Fluorescence quantum yields (ϕ) were estimated by

(12) Zalewski, P. D.; Forbes, I. J.; Seamark, R. F.; Borlinghaus, R.; Betts, W. H.; Lincoln, S. F.; Ward, A. D. *Chem. Biol.* **1994**, *1*, 153.
(13) Taki, M.; Wolford, J. L.; O'Halloran, T. V. *J. Am. Chem. Soc.* **2004**, *126*, 712.
(14) Zhang, X.; Hayes, D.; Smith, S. J.; Friedle, S.; Lippard, S. J. *J. Am. Chem. Soc.* **2008**, *130*, 15788.
(15) Komatsu, K.; Urano, Y.; Kojima, H.; Nagano, T. *J. Am. Chem. Soc.* **2007**, *129*, 13447.
(16) Mikata, Y.; Wakamatsu, M.; Kawamura, A.; Yamanaka, N.; Yano, S.; Odani, A.; Morihiro, K.; Tamotsu, S. *Inorg. Chem.* **2006**, *45*, 9262.
(17) Chimirri, A.; Monforte, A. M.; Monforte, P.; Nicolo, F.; Rao, A.; Zappala, M. *Heterocycles* **2000**, *53*, 613.
(18) Gagne, R. R.; Spiro, C. L.; Smith, T. J.; Hamann, C. A.; Thies, W. R.; Schiemke, A. K. *J. Am. Chem. Soc.* **1981**, *103*, 4073.
(19) *SAINT, SMART and SADABS*; Bruker AXS Inc., Madison, WI, 2001.
(20) Pflugrath, J. W. *Acta Crystallogr.* **1999**, *D55*, 1718.
(21) Sheldrick, G. M. *Acta Crystallogr.* **2008**, *A64*, 112.

integrating the area under the fluorescence curves with the equation

$$\varphi_{sample} = \frac{OD_{standard} A_{sample}}{OD_{sample} A_{standard}} \varphi_{standard}$$

where A is the area under the fluorescence spectral curve and OD is the optical density of the compound at the excitation wavelength.[22] The standard used for the measurement of the fluorescence quantum yield was anthracene (ϕ = 0.36 in cyclohexane).[23]

Imaging System. The imaging system was composed of a fluorescence microscope (ZEISS Axioskop 2 plus) with an objective lens [10× (A375 and HT-29)].

Preparation of Cells. A375 human melanoma and HT-29 human colon cancer cell lines were purchased from National Center for Cell Science, Pune, India, and used throughout the study. Cells were cultured in DMEM (Gibco BRL) supplemented with 10% FBS (Gibco BRL), and a 1% antibiotic mixture containing PSN (Gibco BRL), at 37 °C in a humidified incubator with 5% CO_2. For the experimental study, cells were grown to 80−90% confluence, harvested with 0.025% trypsin (Gibco BRL) and 0.52 mM EDTA (Gibco BRL) in phosphate-buffered saline (PBS; Sigma Diagnostics), plated at the desired cell concentration, and allowed to reequilibrate for 24 h before any treatment. "Cells" were rinsed with PBS and incubated with DMEM-containing **1** (10 μM, DMSO:water = 1:9) for 15 min at 25 °C. All experiments were conducted in DMEM containing 10% FBS and 1% PSN antibiotic.

Cell Cytotoxicity Assay. To test the cytotoxicity of **1**, 3-(4,5-dimethylthiazol-2-yl)-2,*S*-diphenyltetrazolium bromide (MTT) assay was performed by the procedure described earlier.[24] After treatment of **1** (5, 10, 25, 50, 75, and 100 μM), 10 μL of a MTT solution (10 mg/mL PBS) was added in each well of a 96-well culture plate and incubated continuously at 25 °C for 3 h. All media were removed from wells and replaced with 100 μL of acidic isopropyl alcohol. The intracellular formazan crystals (blue-violet) formed were solubilized with 0.04 N acidic isopropyl alcohol, and absorbance of the solution was measured at 595 nm wavelength with a microplate reader. Further, the same experiment was performed with a fixed concentration of the chemosensor (10 μM) and the simultaneous addition of Zn^{2+} and *N*,*N*,*N*′,*N*′-tetrakis(2-pyridylmethyl)ethylenediamine (TPEN). The cell viability was expressed as the optical density ratio of the treatment to control. Values are mean ± standard deviation of three independent experiments. The cell cytotoxicity was calculated as % cell cytotoxicity = 100% − % cell viability.

Results and Discussion

The reaction of 2,6-diformyl-4-methylphenol and 2-(2-aminophenyl)-1*H*-benzimidazole results in the formation of the chemosensor **1** (Scheme 1) in a single step. The single-crystal X-ray structure of **1** (Figure 1) reveals that one of the DBIQ fragments is disordered into two conformations (*Z* and *E*) by rotation about the C(*p*-cresol)−C(quinazoline) bond with occupancy factors 0.654(4) and 0.346(4), respectively. The Zn^{2+}-bound species of **1**, **2**, was obtained by the reaction of **1** with $Zn(NO_3)_2 \cdot 6H_2O$ in the pH range 7.2. X-ray diffraction data for **2** were collected using synchrotron radiation (λ = 0.6889 Å) because of its small crystal size, needle

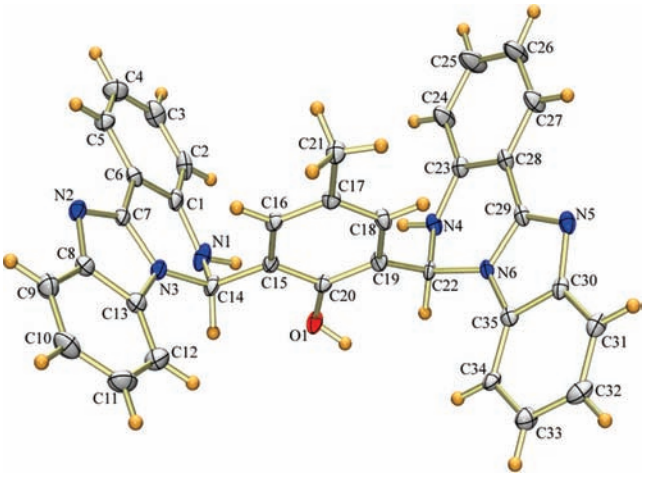

Figure 1. ORTEP diagram (20% probability) of the chemosensor **1** with an atom numbering scheme. DMF, H_2O, and the minor occupancy components are omitted for clarity.

Scheme 1. Structure of **1**

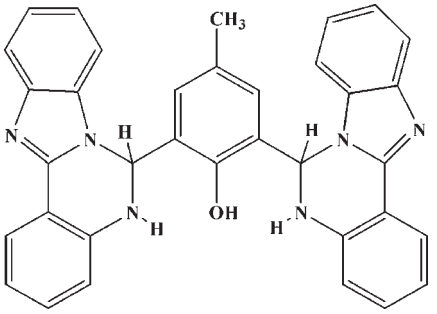

habit, and weak diffraction. The formation of **2** probably needs a [1,5] sigmatropic-type shift of the secondary N−H proton of **1** prior to binding with Zn^{2+} to form a Schiff base structure (Scheme S1 in the Supporting Information), which is evident from the crystal structure of **2** (Figure 2). Because the complex crystallizes as a nitrate species, it will have little relevance to physiological conditions.

X-ray Crystal Structures of 1 and 2. In compound **1**, the central *p*-cresol ring is disubstituted at the 2 and 6 positions by DBIQ ring systems, one of which is disordered into *Z* and *E* conformations with occupancy factors 0.654(4) and 0.346(4), respectively. In all of the conformers, the dihydropyrimidine rings adopt a screw-boat conformation. The dihedral angle between the quinazoline and benzimidazole rings lies in the range 5.8(1)−8.4(6)°, indicating that the DBIQ rings are almost coplanar. The *p*-cresolate ring plane is nearly orthogonal to the DBIQ plane, as indicated by the dihedral angle range of 83.6(6)−85.4(3)°. In the imidazole ring, there is significant shortening of the N2−C7, N5−C29, and N5A−N29A bonds [1.316(3), 1.319(8), and 1.332(15) Å, respectively] and lengthening of the N3−C13, N5−C30, and N5A−C30A bonds [1.400(3), 1.403(7), and 1.411(14) Å, respectively]. This indicates a failure of the delocalized aromatic system, which might be expected for this class of molecules. C7−N2−C8, C29−N5−C30, and C29A−N5A−C30A bond angles are equal to 104.3(2)°, 104.4(6)°, and 104.4(1)°, respectively. The N1−C14 [1.471(3) Å], N4−C22 [1.459(7) Å], and N4A−C22A [1.443(15) Å] bonds and the N1−C14−N3

(22) Austin, E.; Gouterman, M. *Bioinorg. Chem.* **1978**, *9*, 281.
(23) Du, H.; Fuh, R. A.; Li, J.; Corkan, A.; Lindsey, J. S. *Photochem. Photobiol.* **1998**, *68*, 141.
(24) Ratha, J.; Majumdar, K. A.; Mandal, S. K.; Bera, R.; Sarkar, C.; Saha, B.; Mandal, C.; Saha, K. D.; Bhadra, R. *Mol. Cell. Biochem.* **2006**, *290*, 113.

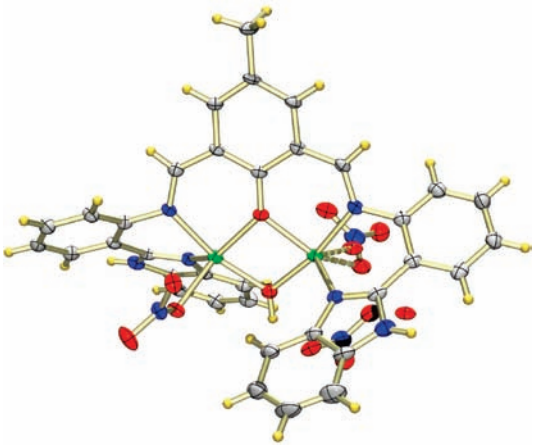

Figure 2. Thermal ellipsoid (20% probability) plot of **2**. Dotted bonds indicate the disordered molecules. Color code: C, gray; O, red; N, blue; Zn, green; H, yellow.

[106.50(18)°], N4−C22−N6 [106.0(6)°], and N4A−C22A−N6A [108.6(11)°] angles illustrate sp^3 hybridization of C14, C22, and C22A, respectively. The supramolecular structure in compound **1** is determined by direction-specific N−H---O interaction, which links the molecules together into chains running parallel to the crystallographic *a* axis. Atom O1 in the molecule at (*x*, *y*, *z*) forms, via H1, a hydrogen bond to N2 in the molecule at (1 + *x*, *y*, *z*) [O1---N2 = 2.747(2) Å, H1---N2 = 1.97 Å, and O1−H1---N2 = 154°], a $C^2_2(8)$ chain that runs parallel to the [1 0 0] axis.

The metal complex **2** is a dinuclear species with a (μ_2-cresolato)(μ_2-hydroxo) core. Both Zn atoms are five-coordinate with N_2O_3 donor sets made up of a bridging μ_2-cresolato O atom, a benzimidazole N atom, an imine N atom, a bridging μ_2-hydroxo O atom, and an O atom of the coordinated nitrate ion/water molecule. The trigonality index parameter τ [$=(\phi_1 - \phi_2)/60$, where ϕ_1 and ϕ_2 are the two largest L−M−L angles of the coordination sphere] has been calculated for the pentadentate Zn sites. The τ values of 0.57 [Zn1] and 0.50 [Zn2] show that the geometries at the metals are intermediate between trigonal-bipyramidal and square-pyramidal geometry (for a perfect square pyramid, τ = 0, and for a perfect trigonal bipyramid, τ = 1). The largest angles at the metals are O2−Zn1−N4 = 168.9(3)° and O2−Zn2−N3 = 164.0(2)°, showing that the O atom (O2) of the exogenous hydroxo bridge is trans to the articular tertiary aminic N atom [N4 and N3] in each case. The Zn−Zn separation is 3.102(2) Å. Incidentally, the Zn−Zn separation of 3.10 Å is similar to bovine lens leucine aminopeptidase, a dizinc-(II)-containing metalloenzyme. The Zn−OH−Zn bridge is slightly asymmetric, with Zn−O distances of 1.951(6) and 1.970(6) Å. The Zn1−O1−Zn2 angle is 96.7(2)°, while the Zn1−O2−Zn2 angle is 104.6(2)°. The N2 atom in the molecule at (*x*, *y*, *z*) forms, via H2A, a hydrogen bond to O7 atom in the molecule at (1 − *x*, 1 − *y*, −*z*) [N2---O7 = 2.818(11) Å, H2A---O7 = 2.03 Å, and N2−H2A---O7 = 151°], producing a $R^2_2(16)$ ring centered at ($^1/_2$, $^1/_2$, 0). Crystal packing of **2** (Figure 3) shows the intermolecular N−H---O hydrogen-bonding interactions. Selected bond lengths and angles of **1** and **2** are listed in Tables S1 and S2 in the Supporting Information, respectively. Relevant crystal data and structure refinement parameters are provided in Table S3 in the Supporting Information.

Fluorescence Properties and Binding Behavior. The emission spectrum of the chemosensor **1** excited at 360 nm exhibits an emission maximum at 425 nm (Figure S3 in the Supporting Information) with a quantum yield of only 0.019. The fluorescence intensity of **1** (1 μM) significantly increases when various concentrations of Zn^{2+} (0.1−3.0 μM) are added (Figure 4), and the fluorescence quantum yield (0.237) increases more than 12-fold. Interestingly, the introduction of other metal ions causes the fluorescence intensity to be either unchanged or weakened.

A metal ion selectivity study (Figure 5) was then performed for **1** to understand this phenomenon under identical experimental conditions. The fluorescence intensity of **1** (1 μM) was unaffected upon the addition of an excess of 10 equiv (10 μM) of Cr^{3+} and Cd^{2+} and a large excess of Na^+, K^+, and Ca^{2+} (100 μM). The fluorescence intensity was diminished upon the addition of several metal ions (10 μM), e.g., Mn^{2+}, Fe^{3+}, Co^{2+}, Ni^{2+}, and Cu^{2+}. Further, tolerance of the fluorescence intensity due to Zn^{2+} (2 μM) in the presence of 10^3 times an excess of various metal ions (100 μM) like Na^+, K^+, Ca^{2+}, Fe^{3+}, Cu^{2+}, and Mn^{2+} has been successfully verified, with no effects on the fluorescence intensities.

Job's plot analysis revealed that **1** forms a 1:2 (**1**:Zn^{2+}) complex with Zn^{2+} (Figure S4 in the Supporting Information), and this is clearly evidenced from the crystal structure of Zn^{2+}-bound species (**2**). To observe the binding interaction with Zn^{2+} in a buffer medium, the binding constant value has been determined from the emission intensity data following the equation[25,26]

$$Y = Y_0 + \frac{Y_{\lim} - Y_0}{2}\left\{1 + \frac{C_M}{C_L} + \frac{1}{K_a C_L} - \left[\left(1 + \frac{C_M}{C_L} + \frac{1}{K_a C_L}\right)^2 - 4\frac{C_M}{C_L}\right]^{1/2}\right\}$$

Y, Y_0, and $Y_{\lim}$ are the recorded fluorescence intensity, fluorescence intensity without the addition of Zn^{2+}, and fluorescence at the limiting value, respectively, where C_M is the target molecule concentration, C_L is the chemosensor **1** concentration, and K_a is the association constant. The following equation was used for the nonlinear least-squares analysis to determine the association constant K_a (Figure 6), and the value of K_a was estimated as 3.1 ($\pm$0.1) $\times$ 10^7 mol^{-1} L. The estimated value of K_a is too high compared with the reported values,[17] and it significantly indicates the strong association of **1** with the zinc ion. This high value is probably due to the formation of a neutral complex of Zn^{2+} with a bridging bimetallic N_4O donor chelating Schiff-base ligand. The limit of detection, corresponding to a 3σ criterion, was found to be 3.5 $\times$ 10^{-8} g L^{-1} for the zinc ion.

The average fluorescence lifetime (τ) of **1** was estimated as 0.822 ns (Figure 7), whereas a shorter average

(25) Valeur, B. *Molecular Fluorescence: Principles and Applications*; Wiley-VCH: Weinheim, Germany, 2002.
(26) Dhara, K.; Saha, U. C.; Dan, A.; Sarkar, S.; Manassero, M.; Chattopadhyay, P. *Chem. Commun.* **2010**, *46*, 1754.

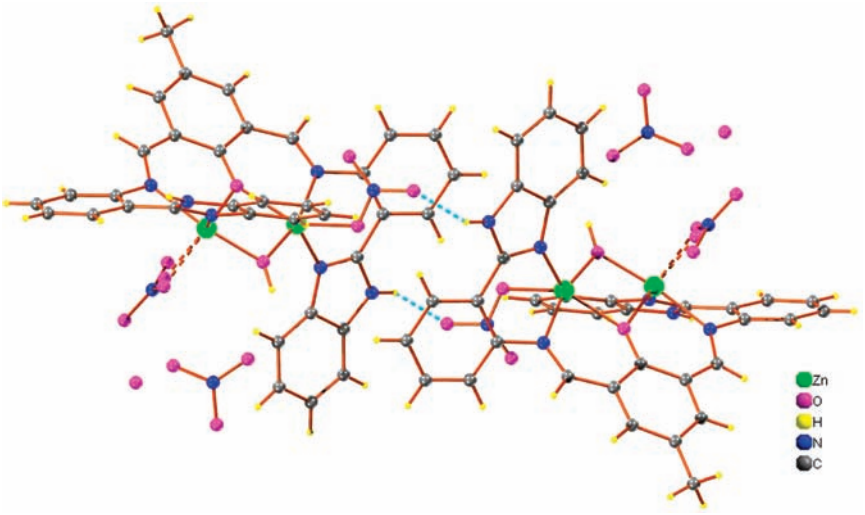

Figure 3. Crystal packing of **2** illustrating the centrosymmetric $R^2_2(16)$ ring formation through intermolecular N−H---O hydrogen-bonding interactions (dotted sky-blue color).

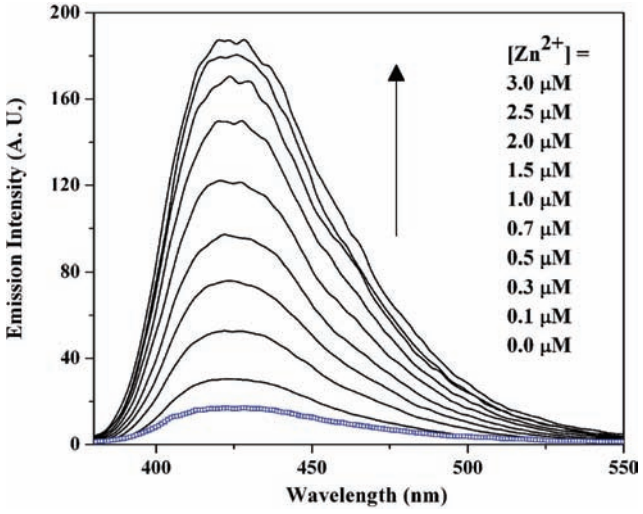

Figure 4. Emission spectra of **1** (1 μM) in the presence of various concentrations of Zn^{2+} in a HEPES buffer [50 mM, DMSO:water = 1:9 (v/v), pH = 7.2] at 25 °C (excitation 360 nm).

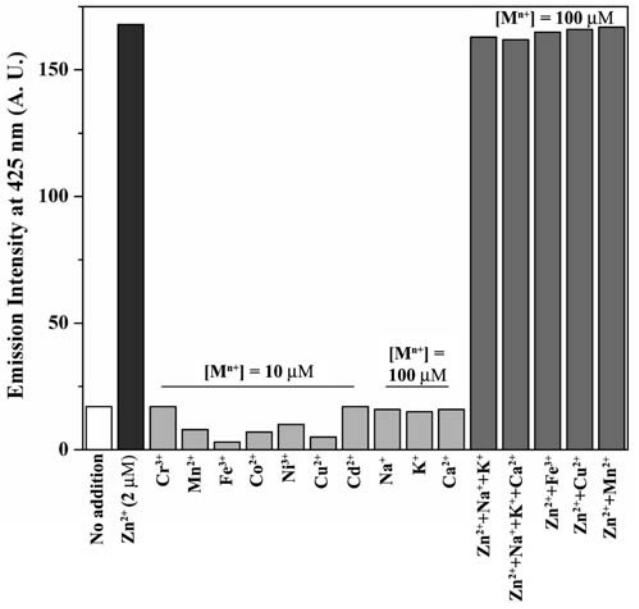

Figure 5. Relative emission intensity change profile of the chemosensor **1** (1.0 μM) in the presence of various metal ions at 25 °C (excitation wavelength: 360 nm) in a HEPES buffer (50 mM, DMSO:water = 1:9 (v/v), pH = 7.2).

fluorescence lifetime (0.200 ns) was detected in the presence of Zn^{2+} (**1**:Zn^{2+} = 1:2). According to the equations[27] $\tau^{-1} = k_r + k_{nr}$ and $k_r = \Phi_f/\tau$, the radiative rate constant k_r and the total nonradiative rate constant k_{nr} of **1** and Zn^{2+}-bound species were calculated and listed in Table S4 in the Supporting Information. The data suggest that the factor that induces fluorescent enhancement is mainly ascribed to the more than 51 times increase of k_r. This enhancement is attributed to the introduction of Zn^{2+} and the strong complexation occurring with **1**, as is evident from the large binding constant value. Upon complexation, the lone pair of electrons on the N atom of the chemosensor **1** is no longer available for PET,[28] leading to fluorescence enhancement.

pH-Dependent Behavior. In addition, we measured the fluorescence intensity of **1** at various pH values in the presence and absence of Zn^{2+}. The fluorescence intensity of **1** decreases under acidic conditions. The chemosensor **1** had a weak fluorescence response to Zn^{2+} in the acidic environment because of protonation of the phenolic hydroxyl[29] and amino groups of **1**, leading to a weak coordination ability of Zn^{2+}.[30] However, satisfactory Zn^{2+}-sensing abilities were exhibited when the pH was increased from 6.0 to 9.0. Thus, **1** displayed good fluorescence sensing ability to Zn^{2+} over a wide range of pH (Figure 8), and the intensity was almost stable around pH = 6.0−9.0, which makes it suitable for application in physiological conditions. These results indicate that **1** can be employed as a selective fluorescent probe to recognize

(27) Turro, N. J. *Modern Molecular Photochemistry*; Benjamin Cummings: Menlo Park, CA, 1978.
(28) Fox, M. A.; Chanon, M. *Photoinduced Electron Transfer*; Elsevier: Amsterdam, The Netherlands, 1988; Parts A−D.
(29) Roy, P.; Dhara, K.; Manassero, M.; Ratha, J.; Banerjee, P. *Inorg. Chem.* **2007**, *46*, 6405.
(30) Liu, Y.; Zhang, N.; Chen, Y.; Wang, L. *Org. Lett.* **2007**, *9*, 315.

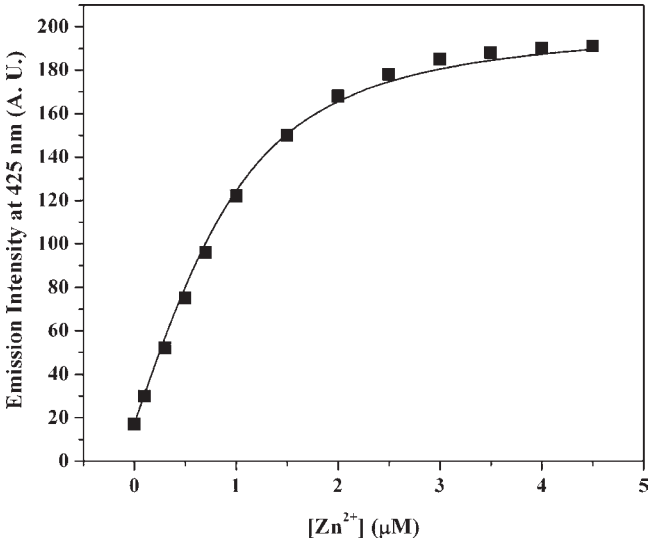

Figure 6. Determination of the association constant K_a.

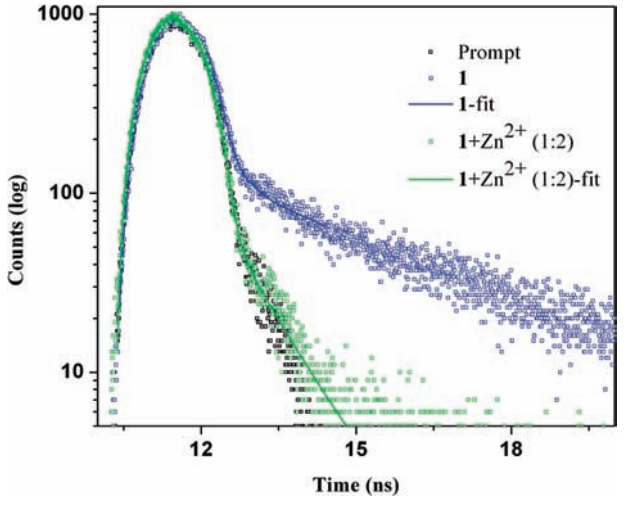

Figure 7. Time-resolved fluorescence decay of **1** in the absence and presence of added Zn^{2+} (λ_{ex} = 372 nm).

and distinguish Zn^{2+} in the presence of various interfering and biologically relevant metal ions.

Absorption Study. The mode of coordination of **1** with Zn^{2+} was investigated by spectrophotometric titration at 25 °C in a HEPES buffer [50 mM, DMSO:water = 1:9 (v/v), pH = 7.2]. Figure 9 illustrates a typical UV−vis titration curve of **1** with Zn^{2+}. As can be seen in Figure 9, the absorption intensity of **1** at 425 nm gradually increased, while the absorption intensity at 362 nm decreased, as the concentration of Zn^{2+} was increased stepwise. This absorption peak is expected to correspond to coordination of **1** with Zn^{2+}. That is, two N atoms in the chemosensor unit coordinated with Zn^{2+} to form a six-membered chelate ring, which consequently extended the conjugated system and resulted in the appearance of the new absorption in the long-wavelength region. The spectra obtained during the stepwise addition showed the appearance of two isosbestic points at ca. 336 and 383 nm. These phenomena illustrated the transformation from free **1** to the Zn^{2+}-coordinated species (**2**). The inset (Figure 9) shows the distribution of data point ΔA ($\Delta A = \Delta A_{\mathbf{1}+Zn^{2+}} - A_{\mathbf{1}}$, where $A_{\mathbf{1}}$ is defined

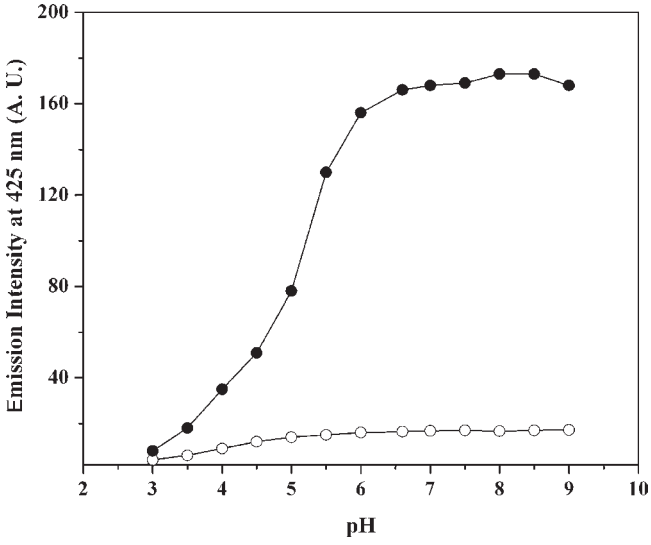

Figure 8. Effect of the pH on the fluorescence intensity of **1** (○; 1 μM) and **1** in the presence of Zn^{2+} (●; 2 μM).

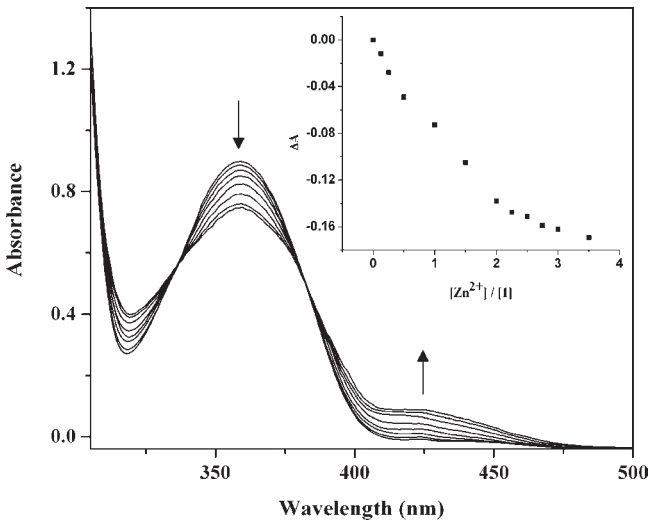

Figure 9. UV−vis spectral changes of **1** (40 μM) upon the addition of Zn^{2+} in a HEPES buffer [50 mM, DMSO:water = 1:9 (v/v), pH = 7.2] at 25 °C, [Zn^{2+}] = 5, 10, 20, 40, 60, 80, 90, 100, 110, 120, and 140 μM. Inset: Absorption changes of **1** at 362 nm upon the addition of Zn^{2+}.

as the absorption intensity of **1** at 362 nm) versus the Zn^{2+}/**1** molar ratio.

Cell Studies. The intracellular Zn^{2+} imaging behavior of **1** was studied on A375 human melanoma and HT-29 human colon cancer cell lines by fluorescence microscopy. After incubation with **1** [10 μM in DMEM, DMSO: water = 1:9 (v/v)] at 25 °C for 15 min, the cells displayed very faint intracellular fluorescence. However, cells exhibited intensive fluorescence when exogenous Zn^{2+} was introduced into the cell via incubation with a $Zn(NO_3)_2$/pyrithione solution (Figure 10). The fluorescence responses of **1** with various concentrations of added Zn^{2+} are clearly evident from the cellular imaging. Moreover, the intensive fluorescence was deeply suppressed by scavenging Zn^{2+} from the cells with the addition of a cell-permeable metal chelator, TPEN (Figure 10). Hence, these results indicate that **1** is an efficient candidate for monitoring changes in the intracellular Zn^{2+} concentration under biological conditions and

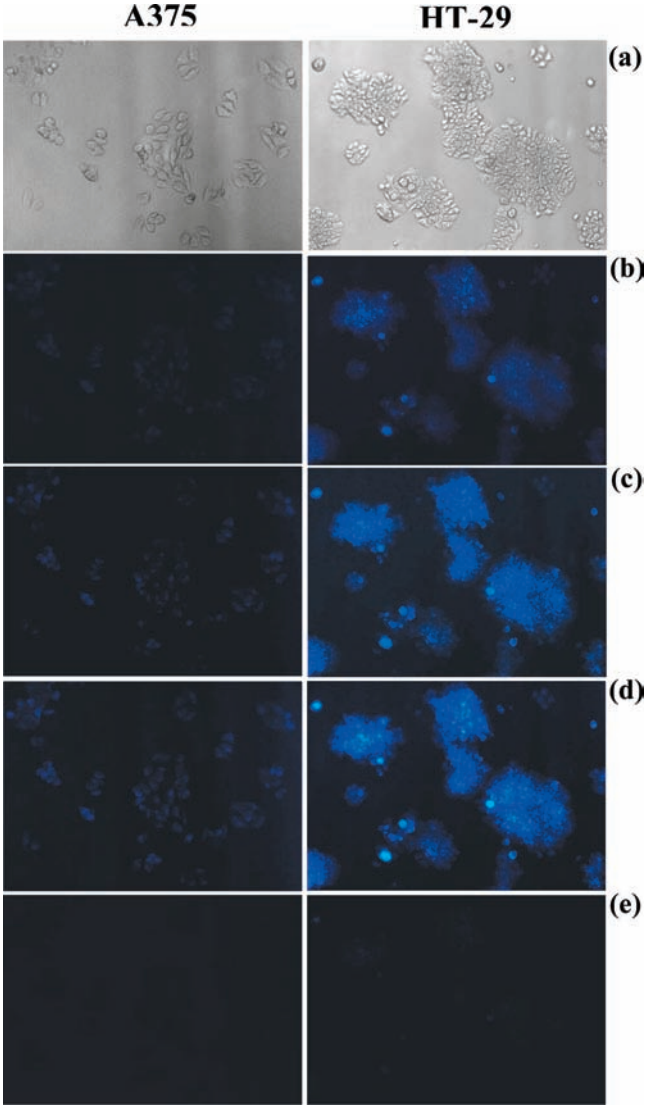

Figure 10. (a) Phase contrast and (b) fluorescence image of A375 and HT-29 cells induced by intracellular Zn^{2+} when incubated with 10 μM **1** for 15 min at 25 °C and washed with PBS. Cells were exposed to pyrithione (pyr, 50 μM) in the presence of sequentially increased concentrations of added extracellular Zn^{2+} as (c) 10 and (d) 20 μM. (e) Return of intracellular Zn^{2+} to the resting level achieved by the addition of TPEN (100 μM). For all imaging, the samples were excited at ~360 nm.

should, therefore, be useful for clarifying the role of Zn^{2+} in biological processes in which the intracellular concentration of Zn^{2+} is important, for example, in cell death induced by ischemia.[31] Although the cell viability measurement might be helpful to calculate the effectiveness of the chemosensor when delivered in various in vivo analyses, **1** should not be cytotoxic at its applied dose and time of incubation.

In order to test its cytotoxicity, we performed MTT assay in both A375 human melanoma and HT-29 human colon cancer cells treated with various concentrations of **1** for up to 3 h. MTT assay, first described by Mosmann,[32] is based on the ability of a mitochondrial dehydrogenase enzyme from viable cells to cleave the tetrazolium rings of the yellow MTT and form a dark-blue formazan crystal, which is largely impermeable to cell membranes, thus resulting in its accumulation within metabolically active, or what are called viable, cells. The number of surviving viable cells is thus directly proportional to the level of the formazan product created. The resulting intracellular formazan can then be solubilized and quantified by spectrophotometric means. MTT assay thus measures the cell proliferation rate and, conversely, when metabolic events lead to cell death because of cytotoxicity, the reduction in cell viability. As shown in Figure S5a (see the Supporting Information), 10 μM **1** did not show significant cytotoxic effects on both A375 human melanoma and HT-29 human colon cancer cells for at least up to 3 h of its treatment although there was significant cytotoxicity for higher doses after 3 h and onward. Further, when the same experiment was carried out with 10 μM **1** and Zn-pyr (50 μM) and finally TPEN (100 μM) (see Figure S5b,c in the Supporting Information) added to the medium for 3−12 h, respectively, a slight reduction in the viability was noted, indicating its cytotoxic effect on A375 and HT-29 cells. This thus suggests that **1** can be readily used for cellular application at the indicated dose and time of incubation without worry about its cytotoxicity.

Conclusions

In conclusion, we have successfully developed a new DBIQ-based fluorescent chemical probe **1**, and it displays high selectivity and sensitivity for Zn^{2+} in a HEPES buffer [50 mM, DMSO:water = 1:9 (v/v), pH = 7.2] at 25 °C. In the presence of Zn^{2+}, significant fluorescence enhancement is achieved, and it is found that the quantum yield was increased more than 12-fold. This is accounted for by formation of the Zn^{2+} complex **2** with a high value of the binding constant. By incubation of cultured living cells (A375 and HT-29) with **1**, intracellular Zn^{2+} concentrations could be monitored through selective fluorescence sensing.

Acknowledgment. Financial assistance from the Department of Science and Technology (DST), New Delhi, India, is gratefully acknowledged.

Supporting Information Available: Scheme S1, Figures S1−S5, Tables S1−S4, and X-ray crystallographic data of compounds **1** and **2** in CIF format. This material is available free of charge via the Internet at http://pubs.acs.org.

(31) Koh, J.-Y.; Suh, S. W.; Gwag, B. J.; He, Y. Y.; Hsu, C. Y.; Choi, D. W. *Science* **1996**, *272*, 1013.

(32) Mosmann, T. *J. Immunol. Methods* **1983**, *65*, 55.